High Brightness AlGaInP Light-Emitting Diodes

Klaus Streubel, Norbert Linder, Ralph Wirth, and Arndt Jaeger

Invited Paper

***Abstract*—This paper reviews the recent progress of AlGaInP high brightness light-emitting diodes. After the discussion of some basic material properties and the general problem of light extraction we will discuss several approaches of high efficiency devices.**

***Index Terms*—AlGaInP, light-emitting diodes, light extraction.**

I. Introduction

THE FIRST COMMERCIAL light-emitting diode (LED) was introduced almost 40 years ago. Since then, the performance of LEDs has been improved continuously with a breathtaking acceleration of progress in the last decade. Today LEDs cover the entire visible color spectrum from blue to red and achieve impressive levels of emission power and conversion efficiencies. The development of very bright visible devices has been enabled by the two material systems AlGaInP for red and yellow and AlGaInN for green and blue. Also organic LEDs as an emerging solution for display applications have made some very significant progress in the recent years. Altogether, the revolutionary development of LED technologies will not only lead to an increased replacement of standard lamps but create a whole range of new applications in our daily life.

AlGaInP materials and devices have led to major advances in high-brightness LEDs. The fabrication of AlGaInP-based light emitters dates back to the mid eighties. It is closely related to the development of metal–organic vapor phase epitaxy (MOVPE) because the standard growth technologies for conventional LEDs like liquid-phase epitaxy (LPE) or hydride vapor phase epitaxy (HVPE) were not suitable for the growth of AlGaInP. The first light-emitting AlGaInP-based devices were semiconductor lasers developed in Japan [1]. High efficiency LEDs grown by MOVPE were reported a few years later [2], [3]. Despite the difficulties in epitaxial growth, the new material system was attractive, because it combined the possibility to achieve high efficiency with the flexibility to tune the emission wavelength over half of the visible spectrum from green to red. Continuous progress in epitaxial growth, processing technology and the design of structures for effective light extraction enabled the fabrication of AlGaInP-LEDs with record high external efficiencies above 50%. The possibility to efficiently generate light in frequently used colors like yellow, orange or red accelerated the use of AlGaInP-LEDs in many applications such as interior and exterior automotive lighting, traffic lights, full color displays, or all kinds of in and outdoor signs.

In this paper, we will briefly review the technology of AlGaInP-based high-brightness LEDs. Starting with a description of some basic material properties such as the band structure, we will then discuss the implications on the internal efficiency of LEDs. Next some general aspects of light extraction from semiconductor structures are discussed. The following sections contain a description of specific technologies for very efficient AlGaInP devices such as surface-structured LEDs, transparent substrate LEDs and other thin-film approaches. This section is concluded with the description of resonant-cavity AlGaInP LEDs which have matured to commercial devices for special applications and offer new aspects and insights in possible future solutions. Finally, we will discuss some reliability issues of AlGaInP LEDs.

II. AlGaInP Alloys

1) Band Structure: The alloy system $(Al_xGa_{1-x})_yIn_{1-y}P$ is, at present, the only direct semiconductor material that is technologically available for a range of colors from red (650 nm) to yellowish-green (560 nm). It has widely replaced the indirect bandgap emitters GaP:N and GaAsP:N in this spectral range, which are limited to a few percent of internal efficiency. For commercial applications the material is almost exclusively grown by MOVPE on misoriented GaAs substrates to avoid ordering [4]. In most LED structures, the layers used are lattice-matched to the substrate in order to obtain low dislocation densities. Since AlP and GaP have nearly identical lattice constants, the In mole fraction $(1-y)$ is close to 0.48 for these alloys, almost independent of the Al and Ga contents.

As usual for Zincblende type lattices, the band structure of the material has a single conduction band with minima at the Γ-, the X- and the L-points, and three valence bands with degenerate heavy and light hole bands at the Γ-point. For low Al-content the bandgap is direct, but becomes indirect with X being the lowest conduction band level for increasing Al-content. The bandgap energies have been determined by various methods [5], yielding slightly different results. A commonly accepted relation for the bandgap variation with composition at room temperature is

$$E_{g\Gamma}(x) = (1.900 + 0.61x)\ \mathbf{eV} \quad (1)$$

$$E_{gX}(x) = (2.204 + 0.085x)\ \mathbf{eV}. \quad (2)$$

Manuscript received December 14, 2001; revised January 22, 2002.

The authors are with Osram Opto Semiconductor, OSSE1, 93049 Regensburg, Germany. (e-mail: klaus.streubel@osram-os.com).

Publisher Item Identifier S 1077-260X(02)03774-7.

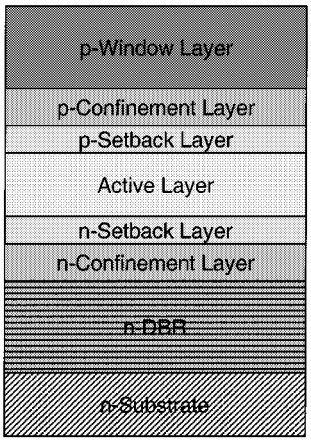

Fig. 1. Schematic drawing of the layer structure of a typical high-brightness LED.

These values indicate that the Γ-X crossover takes place for $x = 0.58$, corresponding to an energy of 2.25 eV or a wavelength of 550 nm. As the crossover composition is approached from the low-energy side, the radiative efficiency of the material decreases drastically due to transfer of electrons from the Γ- to the X-valley, determining the maximum accessible range of wavelengths for LEDs. The conduction L-valley has not been seen directly in any experiment, but has been estimated to be at least 125 meV above Γ_c from experiments involving hydrostatic pressure [5]. Although some theoretical work indicates closer proximity to Γ_c [6], there are negligible effects on the performance of luminescent devices.

Various data indicate that the common 60:40 rule for the conduction and valence band offsets is also applicable in AlGaInP material [7]. The X-minimum of the conduction band changes accordingly, leading to a maximum band offset of about 200 meV in the conduction band. This conclusion has been nicely confirmed by transport experiments on n-i-n heterostructures [8].

2) Internal Efficiency of AlGaInP LEDs: In contrast to standard LEDs such as GaAsP:N, high-efficiency LED structures consist of an elaborate sequence of epitaxial layers (Fig. 1). For the active material, a double heterostructure design or a multiple quantum-well (MQW) structure, embedded between larger bandgap layers, is used to optimize the carrier confinement. Additional setback layers embedded between active layer and confinement layers can be used to control the doping profiles more precisely, since the p-dopants (Mg, Zn) and some n-dopants (Te) tend to diffuse during material growth. Usually, the structures are completed by a top window/current-spreading layer and an optional bottom distributed Bragg reflector (DBR) when grown on GaAs, to recover part of the light emitted in the direction of the GaAs substrate.

The internal electrooptic efficiency of the structure is determined by the balance between radiative recombination and loss processes. Generally, losses can occur through nonradiative recombination processes and carrier leakage across the confinement layers. Spontaneous radiative recombination can be described as a two particle process involving electrons, n and holes, p

$$R_{\rm sp} = B \cdot n \cdot p \tag{3}$$

while the nonradiative recombination rate is given by the Shockley-Read-Hall equation,

$$R_{\rm SRH} = \frac{n \cdot p - n_i^2}{n \cdot \tau_h + p \cdot \tau_e} \tag{4}$$

with B being the radiative recombination constant and τ_e and τ_h the electron and hole capture times. For n≈p, which is the case in most low-doped active layers under operating conditions, $R_{\rm sp}$ changes quadratically with injected carrier concentration, while $R_{\rm SRH}$ depends only linearly on n. Consequently, for low injection densities, corresponding to low operating currents, nonradiative recombination dominates and the optical power is roughly proportional to the square of the current. This changes to a linear relationship when radiative processes start to dominate at higher currents [9].

As the Al-concentration is increased, electrons are thermally transferred from the Γ-minimum to the X-minimum, generating an additional nonradiative recombination channel. Beyond the Γ-X-crossover the radiative efficiency drops to zero. Closed-form expressions for the nonradiative losses through Γ-X-transfer have been derived under certain approximations [7], but a fit to experimental data requires additional assumptions, specifically a reduction of carrier lifetimes with Al-concentration. While this assumption is reasonable (the residual oxygen incorporation, e.g., increases with the Al content), electron leakage and, to a minor extent, hole leakage across the barriers follow a similar relationship on current and temperature, making it difficult to distinguish between the mechanisms in simplified models.

The results of device simulations are shown in Fig. 2(a). Here, the internal efficiency is calculated as a function of the emission wavelength and compared to experimental data on the optical power. The epitaxial structure consists of 40 QWs with a total active layer width of 500 nm and AlInP confinement layers. The nonradiative lifetimes, which are the only free parameters in the calculations, have been chosen such that the calculated quantum efficiencies are in agreement with the ones derived from output power measurements in combination with estimates of the extraction efficiency around 590 nm. As the simulations describe the device data quite accurately, it can be expected that decomposition of the calculated data can give reasonable evidence for the contributions of the various loss mechanisms [Fig. 2(b)]. Here, it is obvious that carrier-leakage supersedes the nonradiative losses, including the X-channel, as soon as the wavelength drops below ∼600 nm. In the red color range (610 nm and larger), on the other hand, the internal quantum efficiency is solely determined by nonradiative recombination processes, i.e., the material quality.

Carrier leakage can be minimized by using larger active layers. Lower carrier densities in the active layer lead to higher effective barriers. At the same time, however, nonradiative processes become more favorable. Thus, the optimum configuration is determined by the material quality and different results have been obtained by different groups [10], [11]. Another way of suppressing the carrier leakage is to increase the barrier heights.

The barriers are maximized by using doped AlInP for the confinement layers. Even larger barriers can be obtained by thin

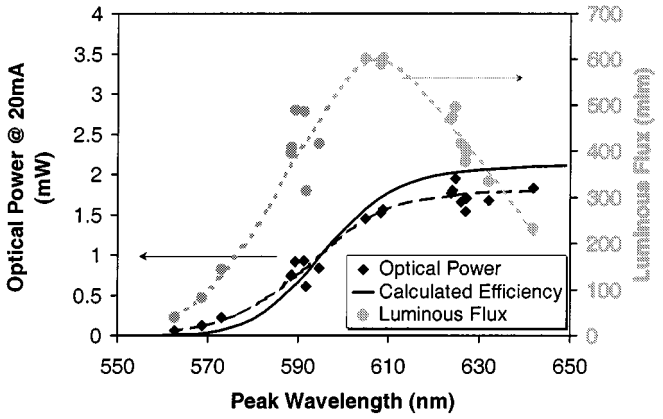

(a)

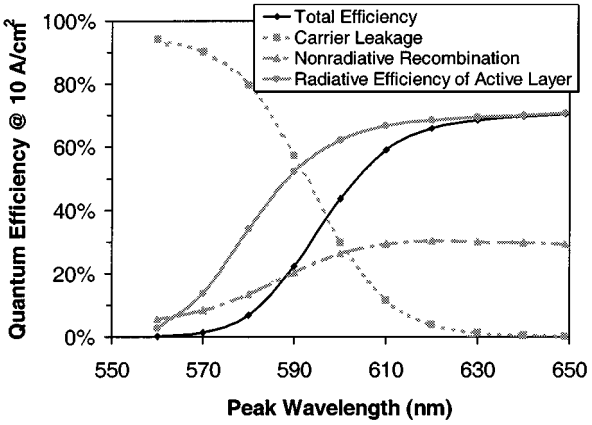

(b)

Fig. 2. (a) Optical output power and luminous efficiencies of high-brightness LED chips at various wavelengths (measured on TO-18 mounts without encapsulation), compared with modeling results. (b) Calculation of loss contributions and radiative efficiencies.

layers of AlInP with tensile strain or multiple quantum barrier (MQB) structures [12]. In the latter case, a combination of barrier layer and short-period strained superlattice (SPSS) is used such that the lowest SPSS miniband accessible for electrons tunneling out of the active layer is above the largest conduction band energy of any of the constituting materials.

III. Light Extraction

1) General: The major problem for high efficiency AlGaInP LEDs is the extraction of light from the semiconductor material into the surrounding media. All materials in the (Al)GaInP–GaAs system show indexes of refraction between $n_2 = 3 \ldots 3.5$. The critical angle for total internal reflection for the transition into a surrounding medium with n_1 is $\theta_c = \arcsin(n_1/n_2)$. Considering a flat interface, the escape cone formed by the rays with $\theta < \theta_c$, and assuming an isotropic spontaneous emission inside the semiconductor crystal, only 2% ($\theta_c = 18°$) or 4% ($\theta_c = 27°$) of the energy emitted inside the semiconductor crystal is extracted into surrounding air or epoxy, respectively.

The common LED structure is a square die cut from a GaAs–AlGaInP epitaxial structure with electrodes on the bottom and top side. In the wavelength range of the AlGaInP emission, the GaAs substrate is not transparent and only the emission into the top escape cone contributes to the extraction efficiency ($c_{\text{ex}} = 0.04$). The top electrode shadows some fraction of the emission and reduces the theoretically possible extraction further. An additional reduction is attributed to current crowding around the top electrode. To partly overcome these problems usually a transparent window layer of some microns thickness is grown on top of the active layers. This results in an improved current spreading and additionally increases the extraction of light through the side facets [13].

Frequently the LED structure is grown on AlGaAs- or AlGaInP-based DBRs to reduce the effect of substrate absorption. However, the angle of acceptance of such a DBR mirror is limited due to the small difference of the index of refraction.

A figure of merit is the integral power reflected from a DBR mirror within the escape cone. For a mirror with the stop band center around 630 nm, $Al_{0.5}Ga_{0.5}As$ and AlAs may be used as high and low index quarter wavelength layers, respectively. Such a DBR with 20 pairs of $Al_{0.5}Ga_{0.5}As$–AlAs has an integral reflectivity of 50% for rays inside the escape cone. A linewidth of 20 nm for emission spectrum of the active layer was assumed for the calculations. The integral reflectivity of the DBR is increased when the stop band center of the DBR is detuned away from the emission wavelength. According to the angular dependence of the DBR properties, off-axis rays are reflected more efficiently if the stop band center is shifted to longer wavelengths. Since the solid angle element increases for off-axis rays the integral reflectivity of the mirror is boosted to an optimum of 80% for a stop band center of 670 nm. For yellow DBRs, integral reflectivities close to 75% can be achieved with properly adjusted compositions and detuning.

Especially for yellow devices, the thickness of the active layers is typically equal or larger than 500 nm. Hence, a part of the rays reflected at the DBR mirrors is absorbed in the active layer, reducing the efficiency of the DBR.

A positive contribution to the extraction efficiency is made by absorption of photons propagating outside an escape cone and reemission into an escape cone. The efficiency of this so-called photon-recycling effect naturally depends on the internal quantum efficiency η_{int}. However, also the thickness l and the absorption coefficient α of the active layer have to be considered. A raytrace calculation of the extraction efficiency for a single escape cone over the optical density $\alpha^* l$ of the active layer is shown in Fig. 3, where the internal quantum efficiency has been varied between 0.25 and 1. As a reference, a calculation without photon recycling has been carried out. Without photon-recycling, only the effect of increasing absorption is observed. When photon recycling is taken into account, a thin active layer is favorable in material with low external efficiency (up to approximately 60%), whereas for efficiencies higher than 80% the effective absorption is reduced significantly and multiple scattering processes occur. Since red AlGaInP-LEDs have high internal efficiencies, thick active layers may be used for such samples. In the yellow wavelength regime, we find low internal efficiencies below 0.5. In terms of extraction efficiency, Fig. 3 implies that a thin active layer should be used in this case. However, the poor carrier confinement in thin yellow active layers necessitates some compromise in terms of an optimum active layer thickness.

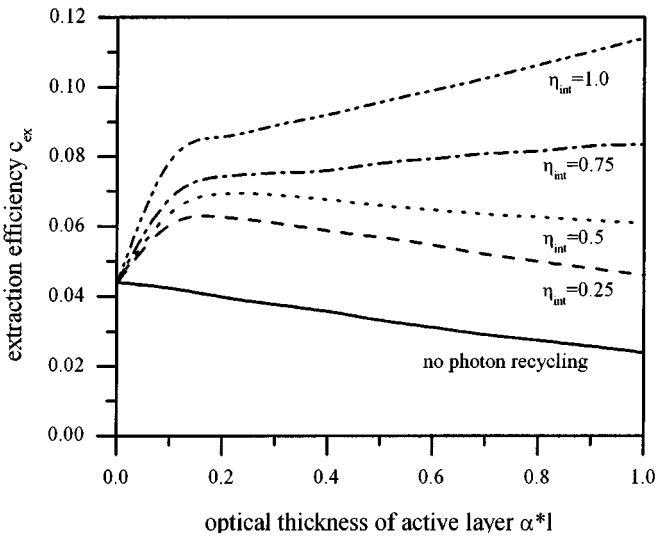

Fig. 3. Extraction efficiency $c_{\rm ex}$ over the optical density $\alpha^* l$ of the active layer. Calculations have been done using a ray tracing model including photon-recycling. A single escape cone and an absorbing substrate was considered.

2) Chip Shaping: Since spontaneous emission is primarily isotropic the most natural way to deal with the problem of total internal reflection is to use a small active volume located in the center of a sphere of semiconductor material. In this case, the rays from the small active volume strike the interface at approximately normal incidence. Variations of this idea are a hemispherical chip, a chip in the form of a Weierstrass sphere, a Paraboloid source or a truncated ellipsoid. Carr [14] calculated the extraction efficiency $c_{\rm ex}$ and radiant intensity for these devices neglecting absorption and allowing single internal reflection at the semiconductor air interface only. For an index of refraction $n = 3.6$ his results show an extraction efficiency of $c_{\rm ex} = 34\%$ for the hemisphere, Weierstrass-sphere and paraboloid source. The truncated ellipsoid has a somewhat lower extraction efficiency of $c_{\rm ex} = 25\%$. The highest radiant intensity is achieved with the Weierstrass-sphere and paraboloid shaped chip. Unfortunately, these devices have not only the most natural chip shape, but are also the most complicated approaches to realize.

Another approach is to break the cubic chip symmetry to give rays that are reflected internally at the semiconductor air interface a second, third or even more chances to alter their direction eventually getting reflected into one of the escape cones. One of these approaches is a truncated cone with the active area near the apex of the cone. In this case, an increased fraction of the radiation is directed by means of reflection at the conical surface toward the flat base of the cone within the escape cone. Carr found maximum extraction efficiency for a half apex angle of $(\pi/2 - \Theta_c)/2$, which is 32° for a typical extraction cone into epoxy with $\Theta_c = 26°$. Assuming a absorbing contact on the apex and no anti-reflection coating Carr found an extraction efficiency of $c_{\rm ex} = 25\%$ into air for this device. However, if the bulk absorption is low, multiple reflections will enhance the extraction efficiency.

IV. Surface-Textured Devices

The simplest way to increase the extraction efficiency is to texture one or more surfaces of the chip. Geometrical structures as described below enhance the number of rays that can penetrate the surface by offering multiple surfaces at different angles of incidence. Another way is to modify the refractive properties of the chip surface by using diffractive structures on top. For an irregular pattern of elements with sizes on the order of the wavelength, the light is scattered isotropically. In this case, an increase of the extraction efficiency of almost 100% has been demonstrated [15]. The full potential of this approach, however, is exploited only for a chip design with an additional wide-angle back reflector, as described below.

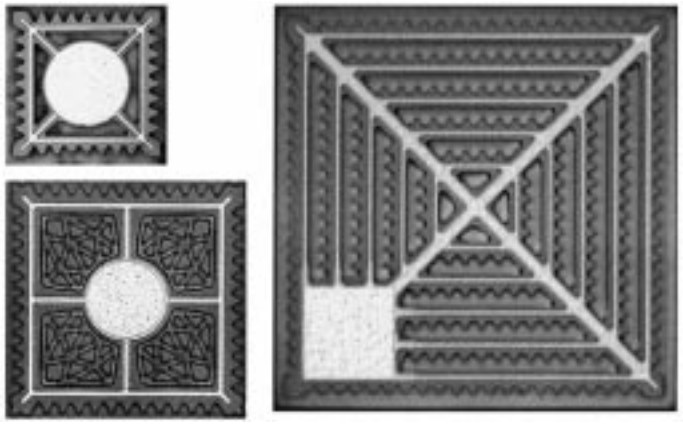

Fig. 4. Top-view images of surface-structured OSRAM chips. Various chip sizes have been fabricated with similar luminous efficiencies, demonstrating the scalability of the concept.

The basic idea of the geometrical surface texturing is to downscale the chip shaping approaches [11]. Geometrical structures with the shape of truncated tetrahedrons are etched into a GaP window layer on top of the active material. In this way, the effective surface area is increased and propagation of rays on closed loops is reduced, leading to enhanced extraction efficiency. In Fig. 4, top-view images of surface structured LEDs are shown. Contact frames are used to distribute the current across the device since current-spreading in the window layer is strongly suppressed underneath the etched structures. Also, current densities are increased in the light extraction structures, enhancing the efficiency further. One advantage of the concept is that it leads to a completely scalable chip design, whereas other advanced extraction mechanisms require certain ratios between chip size and thickness for maximum efficiency. Here, larger chip sizes can simply be obtained by adding more contact frames with attached light extraction structures.

The increase in extraction efficiency depends on the window layer thickness and etch depth. Optical power versus current characteristics are shown in Fig. 5(a) for a device with a 20-μm window. An overall increase of the extraction efficiency of 30% over a rectangular chip is obtained, resulting both from the improved contact geometry and the surface structures. As the window thickness is decreased the advantage becomes larger, leading to, e.g., an improvement of about 60% for a 10-μm window. Luminous efficiencies of more than 30 lm/W have been achieved in a wavelength range from 585 to 625 nm, which is among the best reported for absorbing-substrate LEDs and comes close to the values of transparent-substrate LEDs. The current–light (I–L) characteristics remain linear up to current

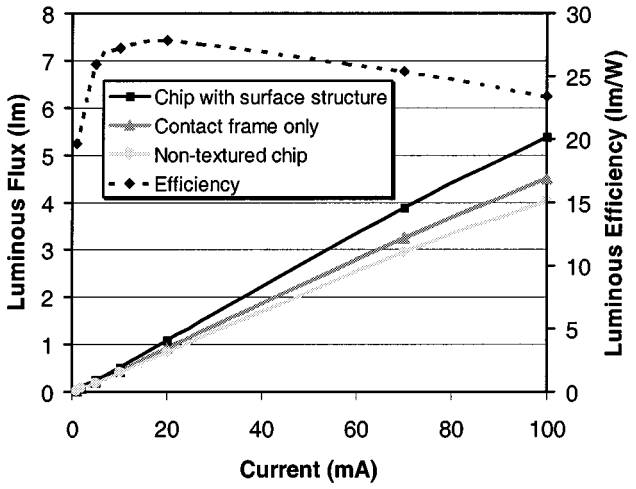

(a)

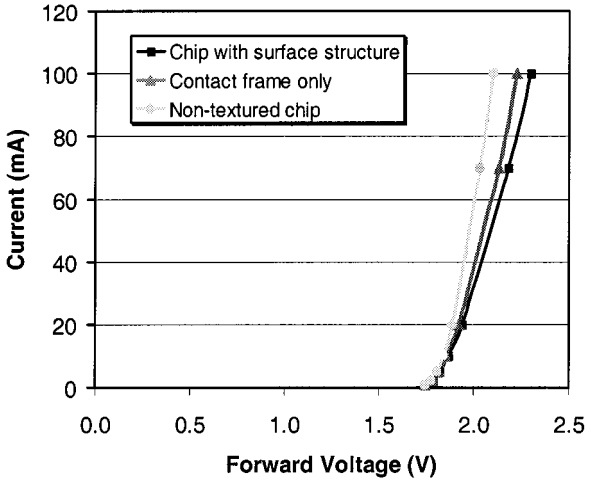

(b)

Fig. 5. *I–L* (a) and current-voltage (b) characteristics of surface-structured OSRAM chips. The chip dimensions are 300 μm $*$ 300 μm.

densities well beyond 100 A/cm^2, which is larger than the usual value for commercial devices. At the same time voltages remain as low as 2.2 V [Fig. 5(b)].

Although increased light extraction through the sidewalls of the surface structures are clearly observed in the image of a LED under operation [Fig. 6(a)], the radiation characteristics of the chip remains almost ideally Lambertian [Fig. 6(b)]. This is a distinct advantage for the package design, since the chip can replace standard square chips in any package, even in applications where the radiation pattern is critical.

V. Transparent-Substrate LEDs

Knowing the good transparency of GaP in the entire range of AlGaInP emission wavelengths, Kish *et al.* developed a technique to remove the absorbing GaAs substrate and to transfer the AlGaInP-LED layers to a transparent GaP wafer [16]. Direct wafer bonding allows the combination of various semiconductor materials more or less independently of their crystallographic lattice constant. In the case of AlGaInP–GaP wafers with up to 2 in diameter can be bonded [17], limited more by the availability of large diameter GaP-wafers than by the technology.

(a)

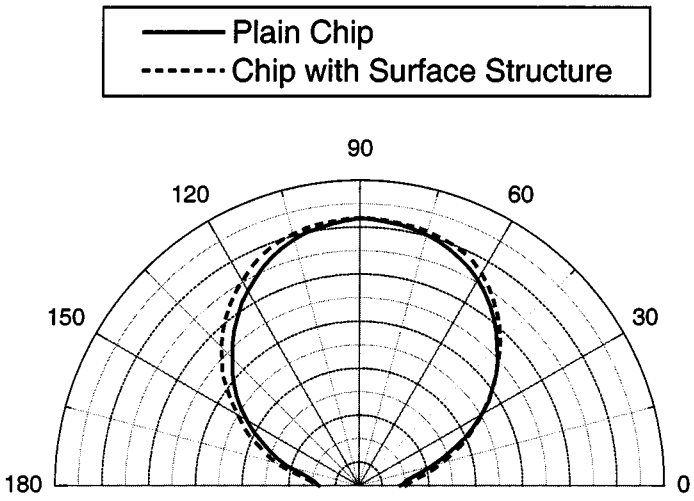

(b)

Fig. 6. Surface-structured chip: (a) Top-view image under operation. (b) Angular radiation characteristics. The radiation pattern is almost exactly Lambertian and deviates little from a standard square chip.

The clean surfaces of both wafers are brought into contact under uniaxial pressure and heated up to temperatures of 750 °C or more [18]. Under such conditions and with proper crystallographic alignment, the two materials form a semiconductor heterointerface with covalent bonds between the two materials. The interface is optically transparent and conducts heat, as well as the electrical current. However, excellent control over this complex process is required in order to achieve low-resistance electrical conductance over the entire bonded area. The feasibility of the AlGaInP-GaP wafer bonding process for the fabrication of a high-volume low-cost device as an LED has been demonstrated by Hewlett-Packard company and is now routinely used in production. The new class of AlGaInP LEDs is named transparent-substrate (TS) LEDs compared to absorbing-substrate (AS) LED on GaAs-wafers.

With the very thick GaP current spreading layer on top of the AlGaInP active region and the transparent GaP-wafer below, the TS-LEDs achieve record high levels of light extraction. For a rough estimation of the extraction efficiency, we can assume that light extraction on all sides of the die is only limited by total internal reflection. Effects like internal absorption, photon recycling and multipass reflections are then neglected. For an encapsulated die, this gives us about 4% extraction on all six sides, which adds up to a total extraction efficiency of 24%. In real AlGaInP TS LEDs, even higher values up to 32% at 630 nm are reported [10]. In terms of luminous efficiency, which takes

the human eye sensitivity into account, the maximum value of 74 lm/W is achieved at shorter wavelengths (615 nm).

The extraction efficiency of TS-LEDs can be further enhanced, if the die is shaped into geometries like cones, pyramids or spheres [14]. The highest reported efficiencies of AlGaInP LEDs are achieved with wafer-bonded TS-material cut into dies with the shape of a truncated inverted pyramid [19]. Light is generated at the base of the pyramid and extracted at a reduced number of reflections and with low photon path length within the semiconductor. The truncated inverted pyramid LED achieved a luminous efficiency of 102 and 68 lm/W at 610 and 598 nm, respectively. A peak external efficiency of 55% was measured at 650 nm.

VI. Thin-Film LEDs

In the following section, we will discuss a number of approaches for high efficiency LEDs which do not rely on direct wafer bonding to GaP-substrates. They all have in common that the AlGaInP structure is at first deposited on GaAs wafers, but the absorbing GaAs is subsequently removed in the fabrication process. Transfer to a new carrier can be facilitated either on chip- or wafer-level and usually involves an intermediate metal layer for soldering. Since the final result is a device in which the thin film of AlGaInP active material has been transferred from one wafer to another, the devices are frequently named "thin-film" LEDs. Compared to TS-LEDs with a basically isotropic emission pattern, thin-film LEDs are more directional top emitters which might be an attractive feature for many applications.

1) Wafer Fused Thin-Film LED: A viable alternative to direct wafer bonding is to solder wafers with an intermediate metal layer. This technology is well known in the silicon world and used, e.g., for the fabrication of micro mechanical components. In the context of AlGaInP-LEDs, the idea is to transfer the epitaxial structure on wafer level to a new carrier by soldering and subsequent GaAs removal. This process generates a new wafer with a metal layer buried between the epitaxial LED layers and the carrier material. For the functionality of the LED, both the high reflectivity of the metal-semiconductor interface as well as the possibility to form ohmic contacts are favorable.

The process flow is shown schematically in Fig. 7. After epitaxial growth, Au and AuSn are deposited on the AlGaInP-LED structure and the carrier wafer, respectively. For simplicity, GaAs was chosen as carrier material because it offers a good electrical conductivity and a comparable thermal expansion to the AlGaInP layers. Carrier and LED-structure are then brought into contact and heated up to 350 °C. At this temperature both metals are molten and Au from the pure Au-layer is diluted in the AuSn alloy increasing the Au–Sn ratio. When the Sn-fraction changes from 30% (weight percent) to about 20%, the process is terminated by cooling down to room temperature. After bonding, the GaAs substrate is removed by selective wet chemical etching. Processing of the "new wafer" is then finished using standard LED processing technology.

Fig. 8 shows the basic principle of an LED based on thin-film technology. The metal layer below the active layer serves both as reflector and p-electrode. Light, which is not directly extracted,

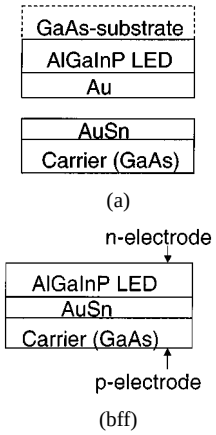

Fig. 7. Schematic layout of the thin-film process sequence. (a) Metal layers of Au and AuSn are deposited on the epitaxial AlGaInP-structure and the carrier wafer, respectively. After bonding and GaAs removal the LED structure together with the new carrier forms an artificial wafer (b) which can be processed using standard LED processing.

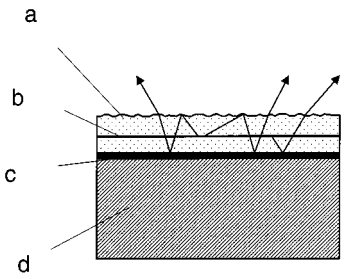

Fig. 8. Principle of operation of an LED with metallic reflector. (a) Rough surface, (b) thin active layer, (c) metallic mirror, and (d) carrier.

is reflected either by total reflection at the semiconductor-air (or epoxy) interface or at the metal mirror. Extraction is significantly enhanced if the reproduction of reflection angles is suppressed, e.g., by surface roughness. Other critical parameters for high efficiency are a sufficiently thin active layer for reduced self-absorption and a power reflectivity of more than 90% at the metal semiconductor interface. Although metals like Au, Al, or Ag offer a very high reflectivity on AlGaInP or AlGaAs, the reflectivity is greatly reduced if the metals are alloyed to form good electrical contacts. Even on highly doped semiconductors contact alloying is necessary to reduce the contact resistance. For the thin-film LED, this problem is solved by locally separating areas with high reflective mirrors from areas with good electrical contacts to the semiconductor. A thin dielectric layer such as Si_2N_3 or SiO_2 is deposited between the semiconductor and the metal layer(s). Openings in this dielectric film define the electrical contacts, whereas the rest of the area serves as dielectric/metallic mirror. The layer system can be alloyed in order to lower the contact resistance without significantly changing the optical properties of the mirror area.

An attractive feature of wafer soldering for LEDs is the possibility to structure one of the surfaces before bonding. Geometrical shapes such as cones, prisms or spheres might be transferred into the AlGaInP-structure (or the carrier surface) by etching before they are covered with metal and embedded inside the LED structure. Generally, most of the geometries that have been used to shape dies in order to enhance the extraction of light [14] can also be buried at the bonded interface of

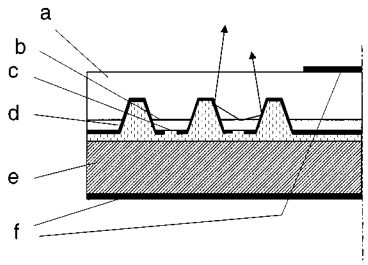

Fig. 9. Schematic cross section of a thin-film LED with buried micro reflectors. (a) AlGaInP-LED structure with removed GaAs-substrate, (b) active layer, (c) electrical contacts, (d) microreflector with dielectric/metal mirror, (e) carrier, and (f) electrodes.

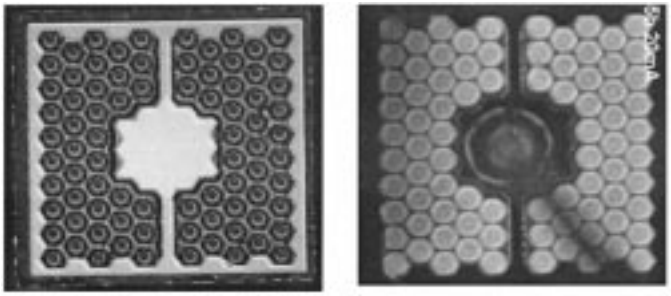

(a) (b)

Fig. 10. Top view (a) and illumination pattern (b) of a 615-nm thin-film LED.

a thin-film LED. An example for an LED with an embedded array of cone-shaped microreflectors is shown in Fig. 9. Truncated cones are etched through the active layer and electrically contacted at the openings in the dielectric layer at the top surface. The fact that the localized current injection leads to a preferred generation of light in the center of the etched cones is used to design the actual shape of the micro structure. Light rays, which are totally reflected at the metal mirror along the cones, are directed upwards toward the LED surface where they are extracted. The path length from the active layer to the top of the LED structure is only a few micrometer and does not include any absorbing material such as the active layer so that the effect of self-absorption inside the device is greatly reduced.

Fig. 10(a) shows the top view of a 615-nm device with a structured interface. Although the array of microreflectors is located underneath the planar top layers, it is clearly visible from the top. Current injection is facilitated from the isolated bond pad and the connected square frame along the edge via the top n-contact layer to the individual p-electrodes in the center of the individual reflectors. As shown in the illumination pattern [Fig. 10(b)] light is generated and extracted around the microreflectors, confirming the principle of operation. Fig. 11 depicts the optical characteristics of the device. Driven at a dc current of 100 mA, the LED emits up to 9.7 lm, corresponding to an optical power around 32 mW. In the range of 10–20 mA of operation current, the luminous performance is above 50 lm/W, with a peak value of 53 lm/W at 10 mA. One of the advantages of the thin-film technology is the low forward voltage that can be achieved. Operated at a dc current of 10 mA, the forward voltage of the 615-nm LEDs is still below 2.0 V.

The devices shown in Figs. 9 and 10 are commercial devices that have been fabricated on full 4-in wafers in a mass-production line at Osram-OS. With these devices, the potential of the thin-film technology for high-brightness LED is certainly not fully exploited. The possibility of shaping the LED surface before bonding offers a whole range of new opportunities to optimize or tailor the device performance by combining novel microstructures for light extraction with new schemes for current injection, heat dissipation, or emission profiles. Fig. 12 shows the luminous performance of another 615-nm thin-film LED which employs a different design of micro reflectors. A peak efficiency of 62 lm/W is achieved around 2 mA, corresponding to a wall-plug efficiency of 23.6%.

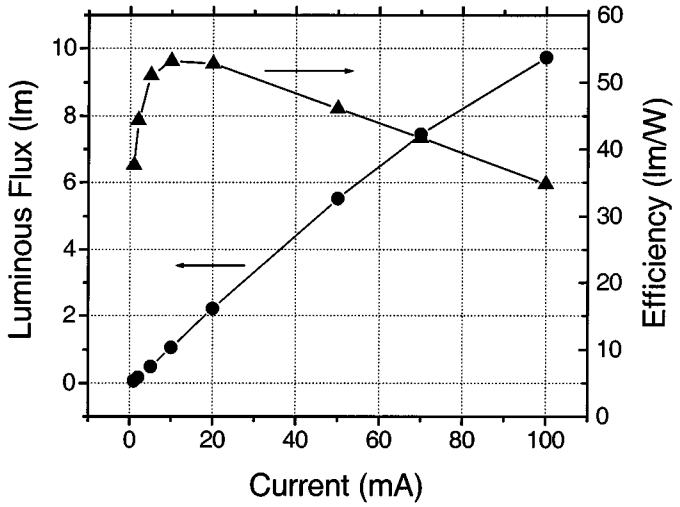

Fig. 11. Optical performance of a 615-nm thin-film LED operated under dc-conditions.

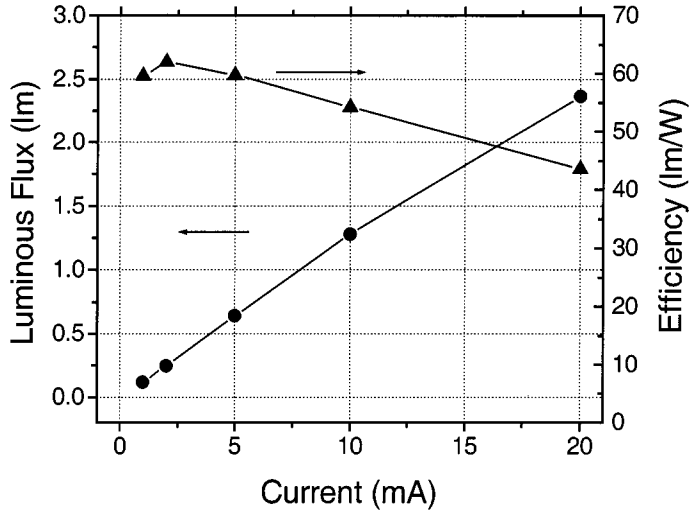

Fig. 12. Characteristics of a 615-nm thin-film LED. The device achieves a maximum efficiency of 62l m/W and emits 2.4l m of optical power at 20-mA dc-current.

A different approach to fabricate thin-film AlGaInP-LEDs is to bond the epitaxial structure to an isolating wafer. In this case, two top electrodes are required. Horng *et al.* fabricated 600–620-nm AlGaInP LEDs on Si-wafers coated with SiO_2 [20], [21] using a metal combination of Au and AuBe for bonding. Despite the intermediate dielectric layer, the LEDs benefited from the good thermal properties of Si. A luminous intensity of 90 and 205 mcd (620 nm) was demonstrated at 20 and 50 mA of operation current, respectively.

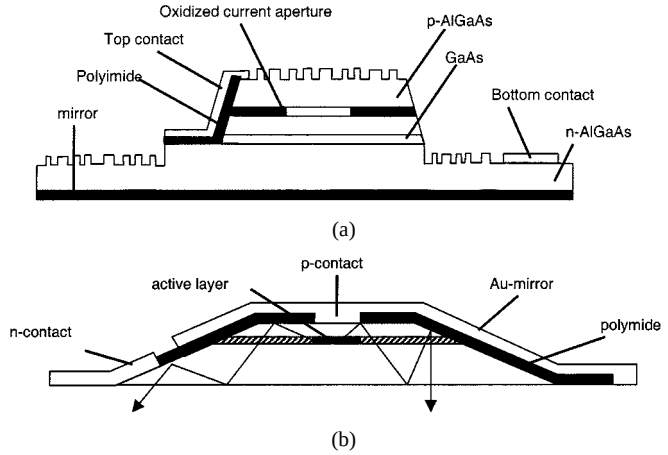

Fig. 13. (a) Nonresonant LED with metallic back mirror and roughened surface. (b) LED with a radial tapered waveguide.

2) Non-Resonant LED: The idea of the NRC-LED dates back to the early 1990's, when Schnitzer *et al.* demonstrated an external efficiency as high as 72% on an optically pumped thin-film LED [22], and shortly later, an electrically pumped device with an external efficiency of approximately 30% [23]. The devices are based on two new techniques for LEDs: "epitaxial liftoff" (ELO) [24] and surface roughening by "natural lithography" [25]. The idea of the ELO process is to insert a sacrificial layer, typically some ten nanometers of AlAs, between the LED structure and the substrate.

A selective wet chemical etching process removes the sacrificial layers and separates the epitaxial layers from the GaAs substrate. Subsequently the thin epitaxial film is transferred to a new wafer by van-der Waals bonding [26]. A metal film on the carrier serves as a highly reflective back mirror for the LED. Surface roughening is achieved by depositing a monolayer film of randomly ordered polystyrene spheres on the LED wafer. The pattern is transferred into the LED surface by dry etching.

The principle of the NRC LED is to randomize the angles of totally reflected light at the top surface with the high reflectivity of a metallic back mirror on the bottom side (Fig. 8). Light which is not extracted through the surface is reflected back and forth between the back mirror and the rough surface. For high efficiency devices, the losses per round-trip through the LED structure have to be minimized by 1) reducing the thickness of all absorbing layers including the active layer and 2) optimizing the reflectivity of the back mirror. Both can be achieved relatively easily in the AlGaAs–InGaAs–GaAs material system. The band structure offers a sufficiently high carrier confinement to use only a few nanometers of active material for efficient light generation. Additionally the reflectivity of common metals like Au, Ag, or Al is very high in the infrared regime.

The combination of epitaxial liftoff and surface roughening has been optimized by Windisch *et al.* on 850-nm LEDs [27], [28]. A schematic layout of the device is shown in Fig. 13(a). The LED employs a mesa structure with a selectively oxidized current aperture to prevent the generation of light under the metal contact. Current injection is facilitated via a annular top-side p-contact and a lateral n-contact around the mesa. In order to extract some of the laterally guided light, not only the surface on top of the mesa but also the area between mesa and bottom contact was roughened. Very high quantum efficiencies of up to 43% and 54% were achieved before and after encapsulation at current densities between 500 and 1000 A/cm^2. Similar devices at 650-nm emission wavelength resulted in 24% quantum efficiency (31% after encapsulation) [29]. Due to relatively high forward voltages, the wall-plug efficiency of these LEDs ranges between 10–15% at 1 mA of operation current.

3) LED With Tapered Waveguide: A device which extracts solely the laterally guided modes inside the epitaxial structure is the LED with a radial tapered output coupler [30] shown in Fig. 13(b). The circular device structure comprises a central top contact, a circular symmetric out-coupling taper with the shape of a shallow truncated cone and a ring-contact along the taper perimeter. Light extraction occurs through the bottom side, where the GaAs substrate has been removed by wet chemical etching.

The principle of operation is to generate light in a small active area, defined by the geometry of the p-contact and to guide it radially toward the tapered area. The dimensions are chosen such that the light rays that hit the taper surface have a small azimuthal wave vector component which is an essential design parameter for efficient light extraction. Light which is reflected at the out-coupling surface is reflected again at the metal mirror on the taper and returns under a more favorable angle of incidence. The procedure is repeated until finally the angle of incidence falls within the escape cone. Absorption inside the waveguide layers which include not pumped active material, and a reflectivity below 100% at the metal mirror on the taper limit the efficiency of this device.

With one and two InGaAs–GaAs compressively strained quantum wells (QWs) as active material emitting at 980 nm, Schmid *et al.* demonstrated 45% of quantum efficiency on encapsulated devices. Maximum efficiency was reached at injection of 2 mA of electrical current and a forward voltage around 2 V. This resulted in a wall-plug efficiency of 30% and 44% before and after encapsulation, respectively. The first attempt to apply the same technology to 650-nm GaInP–AlGaInP devices resulted in a external efficiency of 13% [31].

VII. Resonant-Cavity Light Emitting Diodes

A completely different approach to handle the problem of light extraction is that of a resonant-cavity light-emitting diode (RCLED). Purcell stated in 1946 that the characteristics of the spontaneous emission of an atom is not completely independent of its surrounding environment [32]. In fact, the local strength of the electromagnetic modes and the density of states may change the angular distribution and the emission rate observed. It was proposed in 1992 by Schubert *et al.* [33] to use a resonant-cavity for a LED, and hence redesign the characteristics of spontaneous emission.

In a RCLED, a resonator is used to form the spontaneous emission in such a way, that more of the active layers emission is launched into the escape cone. Because of the Fabry–Pérot resonances, specific wavelengths are allowed for certain directions only.

Such a one-dimensional microcavity is the most simple realization of a photonic band structure. A detailed theoretical analysis of the properties of RCLEDs may be found for example in the articles of Benisty *et al.* [34], [35]. The most important findings to design a high efficiency RCLED are: 1) the cavity order should be as low as possible. Hence, the highest available index contrast for the DBR mirrors forming the resonator should be applied, reducing the penetration depth into the mirror; 2) the active layer should be detuned to the short wavelength side with respect to the cavity resonance. This is not only to compensate for temperature shifts—as in the case of vertical-cavity surface-emitting lasers (VCSELs), but also to increase the amount of extracted light: the solid angle element for the off-axis modes is larger than for the exactly tuned mode; and 3) the QWs of the active layer have to be moved into a maximum of the standing wave inside the resonator.

In the recent years, infrared RCLEDs including metal mirrors and Al_xO_y–GaAs DBR have been demonstrated [36]. Devices using a metal mirror on one side and a $Al_xGa_{(1-x)}As$–GaAs DBR yielded record external quantum efficiencies around 20% [37].

In the red wavelength regime, highly reflective ohmic metal mirrors are very hard to achieve. Those devices usually employ epitaxally grown mirrors [38]–[41].

Following this approach we have been able to achieve a record efficiency of 12.0% for red RCLEDs by fine tuning the structure (Fig. 14). The epitaxial growth included the deposition of a 34 period $Al_{0.5}Ga_{0.5}As$–$Al_{0.95}Ga_{0.5}As$ n-mirror and an undoped active region of five 1% compressively strained 5-nm thick QWs and $(Al_{0.5}Ga_{0.5})_{0.51}In_{0.49}P$ barriers. $Al_{0.51}In_{0.49}P$ confinement layers were employed to maximize the p-barrier height for the electrons. The symmetric active region has a thickness of $\approx$200 nm forming a 1-λ-cavity with the QWs in the anti-node of the electric field. The structure was completed by a C-doped top DBR and a highly doped 10-nm-thick GaAs contact layer.

Large-area devices with an active area of (700 μm)^2 and (300 μm)^2, respectively, as well as a type designed for plastic-optical fiber (POF) communication with a 80-μm-wide current confinement structure [42] have been processed as follows.

An AuZn-contact grid was formed by liftoff. Subsequently, proton implantation was used to define an 80-μm-wide current confining aperture for the POF-type device. Finally, the chip-process was completed by the deposition of TiPtAu bond pads and AuGe n-contacts on p- and n-side of the thinned wafers. After dicing, the RCLEDs were mounted on TO-18 headers for characterization.

Fig. 14 shows the wall-plug efficiency $\eta_{\rm wp}$ and the optical output power $P_{\rm opt}$. For the (700 μm)^2-device, we achieved a maximum wall-plug efficiency of $\eta_{\rm wp} = 12.0\%$ at $I_f = 20$-mA and $U_f = 1.75$-V. The (300 μm)^2-device yielded $\eta_{\rm wp} = 10.2\%$ at $I_f = 10$ mA and $U_f = 1.83$ V.

The POF-type devices are slightly less efficient $(\eta_{\rm wp} = 9.5\%)$. The main reason is that in a large area device, photons, which primarily have been emitted in guided modes propagating along the epitaxial layers, may be absorbed and re-emitted again [43]. This is less probable in the POF type design since the optical paths inside the current confining aperture are shorter. Outside of the aperture, where the current density is negligible, and hence the radiative emission probability is very low, all the light propagating in guided modes is lost.

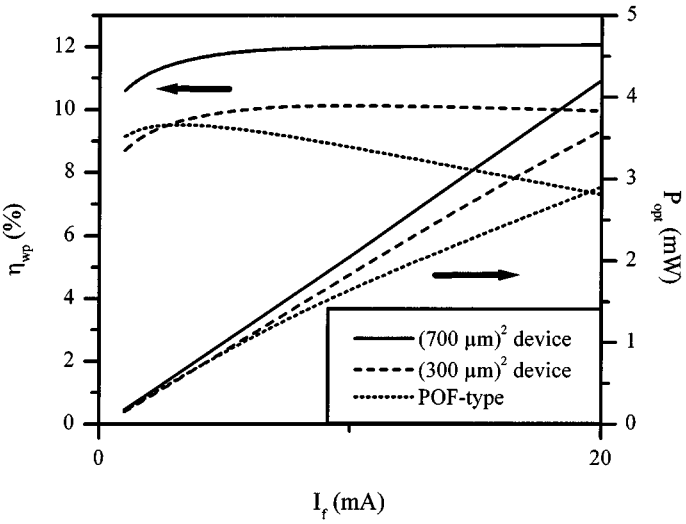

Fig. 14. Wall-plug efficiency $\eta_{\rm wp}$ and optical output power $P_{\rm opt}$ for different chip sizes. These dc measurements have been carried out on TO18 mounts with epoxy encapsulated devices using an integrating sphere.

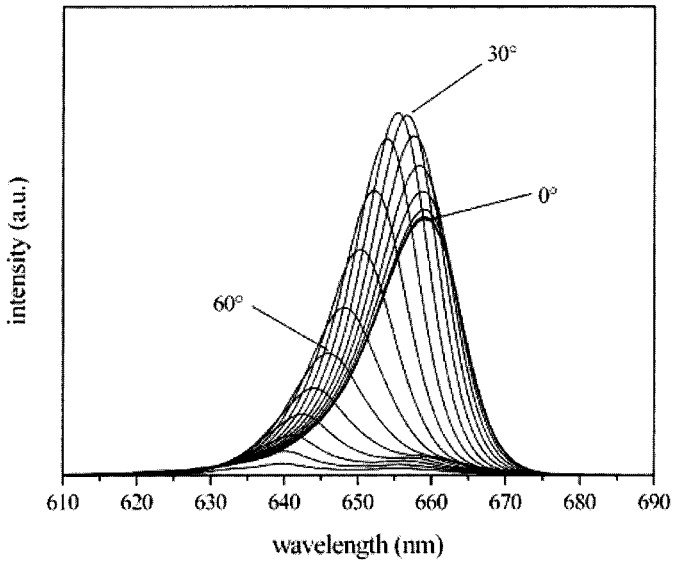

Fig. 15. Emission spectra of a RCLED under different angles. In the forward direction (0°) the long-wavelength part of the QW emission is seen, whereas the shorter-wavelength parts of the spectrum are observed at off-axis angles. When measured in an integrating sphere, a 18-nm-wide spectrum (FWHM) is seen.

In Fig. 15, emission spectra of a RCLED without epoxy encapsulation seen from different angles are displayed. The detuning between QW emission and cavity resonance is adjusted to approximately 12 nm, resulting in maximum intensity at 35° off-axis angles. The long wavelength part of the QW luminescence is emitted into the forward direction, whereas the short wavelength part is emitted under more oblique angles, emphasizing the wave optical nature of the device.

VIII. Reliability

One of the main advantages of AlGaInP LEDs besides record high luminous efficiency in the red to yellowish green

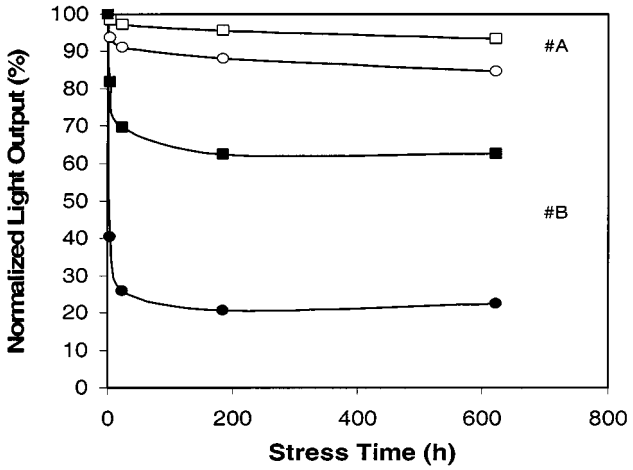

Fig. 16. Normalized light output versus stress time for LEDs with different p-spacer thickness. LEDs were operated at dc current of 50 mA, while the light output is shown for measuring currents of 10 mA (squares) and 1 mA (circles). Degradation is significantly reduced in LEDs with thick p-spacer (open symbols, LED A).

spectral range is the considerably improved reliability compared to competing conventional incandescent bulbs. This fact was demonstrated by several groups [7], [44], [45]. By extrapolating long-term reliability data lifetimes of more than 10^5 hours have been calculated. The reported lifetimes of LEDs compare well with low degradation rates of AlGaInP red laser diodes [46]–[50].

The excellent degradation behavior of AlGaInP lasers has been attributed to a decreased sensitivity of the devices to oxidation due to reduced Al content in the active zone if compared to AlGaAs devices. Also, growth and mobility of dark line defects is decreased owing to incorporation of In in the compound [50].

However, high reliability requires an optimized epitaxial growth. This is demonstrated by AlGaInP LEDs with a different thickness of an undoped spacer layer between the p-type AlInP and the undoped active AlGaInP MQW region. Devices A and B having a spacer layer thickness of 810 and 470 nm, respectively, emit at 615 nm and yield similar high luminous efficiencies. Both devices were stressed at room temperature and a dc current of 50 mA. Nevertheless, Fig. 16 shows a dramatically reduced light output of LED B upon aging as compared to a nearly stable LED A. This different aging behavior is attributed to an increase of nonradiative recombination processes in the active layer of LED B during operation. Generated defects can be identified from the light-current characteristics as a broadening of its nonlinear range, i.e., they reduce light output most effectively in the low-current region of the characteristics [9]. At higher currents this recombination channel is saturated and the effect of the increased nonradiative recombination is no longer observed. This can be recognized in Fig. 16 where degradation curves of LED B are plotted for different measuring currents. Whereas the light output at 1 mA fell to 20% at 10 mA a moderate decrease to 60% is measured. The stable LED A exhibits at the same time only slightly reduced light outputs which are about 90% of the values of the fresh device.

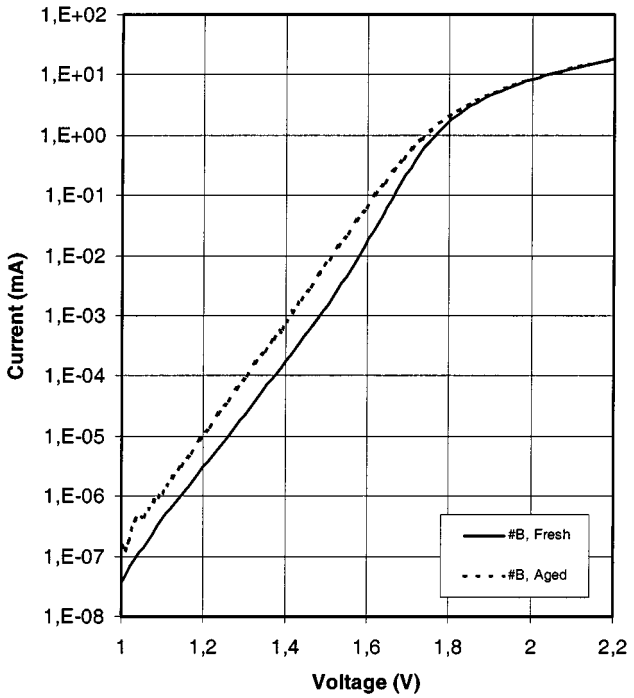

Fig. 17. I–V characteristic of LED B before and after stress at room temperature and a dc current of 50 mA for 622 h. Defect creation upon aging generates an additional electric current component observable as a current increase in the low-voltage region.

The broadening of the nonlinear range of the L–I characteristics is accompanied by a shift to higher currents in the current-voltage (I–V) characteristics [9]. The I-V characteristics of LED B before and after aging are shown in Fig. 17. Three characteristic regions of diode operation are discernible. At low voltages the current is dominated by nonradiative recombination in the space charge region resulting in a diode ideality factor n of about two. As the voltage becomes larger than about 1.6 V, the injected carriers spread all across the active layer and radiative processes become dominant. The ideality factor is now close to one. Finally, the ohmic series resistance determines the I–V characteristic at the highest voltages. Due to defect generation in the active layer the characteristic of the aged device shifted to higher currents at low voltages as compared to the fresh device. This process generates an additional electric current component which becomes less pronounced in the high-voltage regime since the radiative recombination is dominating the nonradiative. Thus the influence of the increased defect density is observed most distinctly in the low-voltage region.

The typical range of driving currents for LEDs is 1–100 mA, where the $n = 1$ current dominates the I–V curve, and the L–I curves are approximately linear. The example above demonstrates not only the importance of a well-controlled epitaxial process, but also the usefulness of testing degradation behavior of LEDs at low measuring currents where nonradiative recombination processes in the active region are more effective. Moreover, this effect is of great importance for applications where high-brightness LEDs are to be dimmed by current. Applications such as LED displays are especially sensitive to a current-dependent degradation of its emitters and tough reliability requirements have to be satisfied.

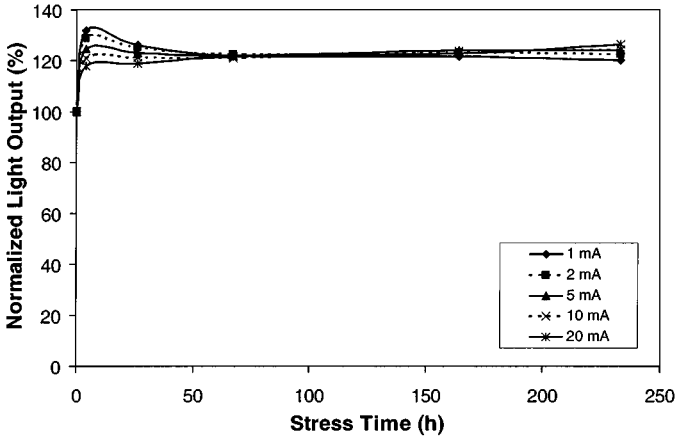

Fig. 18. Normalized light output versus stress time for a thin-film LED. No significant degradation occurs even at low measuring currents.

In the previous chapters, different AlGaInP LED designs have been presented and discussed in detail. Each of them has to be tested with respect to long-term reliability. Fig. 18 displays degradation curves of a thin-film LED emitting at 615 nm. Again the device was stressed at room temperature and a dc current of 50 mA. Except for a small increase of light output during the first hours of stress time, excellent aging behavior even at low measuring currents is observed indicating precise control of the fabrication process for this kind of device.

IX. Summary

Much progress has been made in AlGaInP technology resulting in LEDs with conversion efficiencies comparable to semiconductor laser diodes. The highest efficiencies are achieved using sophisticated processing technologies such as wafer bonding, surface structuring or thin-film processes which will be further improved for high yields and economic mass production. AlGaInP LEDs will become even more pervasive as the costs/photon ratio continues to decrease. Although the devices are already very efficient, we can expect further significant advances in AlGaInP technology that will lead to even better devices in terms of efficiency, costs and lumen output. This will enable new applications and guarantee a bright future for high brightness solid-state lamps.

Acknowledgment

The authors would like to thank their co-workers P. Stauss, C. Karnutsch, I. Pietzonka, S. Tahler, W. Wegleiter, S. Illek, A. Plössl, R. Windisch, and W. Schmid at Osram-OS for some of the results used in this paper and the stimulating discussions. They would also like to thank M. Kuttenberger for her help with the manuscript.

References

[1] K. Kobayashi, "Room-temperature CW operation of AlGaInP double-heterostructure visible lasers," *Electron. Lett.*, vol. 21, pp. 931–932, 1985.

[2] C. Kuo, R. Fletcher, T. Osentowski, M. Lardizabal, M. Craford, and V. Robbins, "High performance AlGaInP visible light-emitting diodes," *Appl. Phys. Lett.*, vol. 57, pp. 2937–2939, 1990.

[3] H. Sugawara, M. Ishikawa, and G. Hatakoshi, "High-efficiency InGaAlP/GaAs visible light-emitting diodes," *Appl. Phys. Lett.*, vol. 58, pp. 1010–1031, 1991.

[4] *Handbook of Semiconductors*, vol. 3, 1995.

[5] A. Meney, A. Prins, A. Philips, J. Sly, E. O'Reilly, D. Dunstan, A. Adams, and A. Valster, "Determination of the band structure of disordered AlGaInP and its influence on visible laser characteristics," *IEEE J. Quantum Electron.*, vol. 1, pp. 697–706, 1995.

[6] K. Brennan and P. K. Chiang, "Calculated electron and hole steady-state drift velocities in lattice matched GaInP and AlGaInP," *J. Appl. Phys.*, vol. 71, pp. 1055–1057, 1992.

[7] F. Kish and R. Fletcher, "AlGaInP light-emitting diodes," in *Semiconductors and Semimetals, High Brightness Light Emitting Diodes*, G. B. Stringfellow and M. G. Craford, Eds., 1997, vol. 48, pp. 149–220.

[8] A. P. Morrison, J. D. Lambkin, C. J. Poel, and A. Valster, "Electron transport across bulk (AlGa)InP barriers determined from the I–V characteristics of n-i-n diodes measured between 60 and 310 K," *IEEE J. Quantum Electron.*, vol. 36, pp. 1293–1298, Nov. 2000.

[9] O. Pursiainen, N. Linder, A. Jaeger, R. Oberschmid, and K. Streubel, "Identification of aging mechanisms in the optical and electrical characteristics of light-emitting diodes," *Appl. Phys. Lett.*, vol. 79, pp. 2895–2897, 2001.

[10] N. F. Gardner, H. C. Chui, E. I. Chen, M. R. Krames, J.-W. Huang, F. A. Kish, S. A. Stockman, C. P. Kocot, T. S. Tan, and N. Moll, "$1.4\times$ efficiency improvement in transparent-substrate $(Al_xGa_{1-x})_{0.5}In_{0.5}P$ light-emitting diodes with thin (<2000 Å) active regions," *Appl. Phys. Lett.*, vol. 74, pp. 2230–2232, 1999.

[11] N. Linder, S. Kugler, P. Stauss, K. P. Streubel, R. Wirth, and H. Zull, "High-brightness AlGaInP light-emitting diodes using surface texturing," in *Proc. SPIE*, vol. 4278, 2001, pp. 19–25.

[12] S. J. Chang, C. S. Chang, Y. K. Su, P. T. Chang, Y. R. Wu, K. H. Huang, and T. P. Chen, "AlGaInP yellow-green ligth emitting diodes with a tensile strain barrier cladding layer," *IEEE Photon. Technol. Lett.*, vol. 9, pp. 1199–1201, 1997.

[13] D. A. Vanderwater, I.-H. Tan, G. E. Höfler, D. C. Defevere, and F. A. Kish, "High-brightness AlGaInP light emitting diodes," *Proc. IEEE*, vol. 85, pp. 1752–1764, 1997.

[14] W. N. Carr, "Photometric figures of merit for semiconductor luminescent sources operating in spontaneous mode," *Infrared Physics*, vol. 6, pp. 1–19, 1966.

[15] R. Windisch, C. Rooman, S. Meinlschmidt, P. Kiesel, D. Zipperer, G. H. Döhler, B. Dutta, M. Kuijk, G. Borghs, and P. Heremans, "Impact of texture-enhanced transmission on high-efficiency surface-textured light-emitting diodes," *Appl. Phys. Lett.*, vol. 79, pp. 1–3, 2001.

[16] F. A. Kish, F. M. Sterakna, D. C. DeFevere, D. A. Vanderwater, K. G. Park, C. P. Kuo, T. D. Osentowski, M. J. Peanasky, J. G. Yu, R. M. Fletcher, D. A. Steigerwald, and M. G. Craford, "Very high-efficiency semiconductor wafer-bonded transparent-substrate $(Al_xGa_{1-x})_{0.5}In_{0.5}P$/GaP light-emitting diodes," *Appl. Phys. Lett.*, vol. 64, pp. 2839–2841, 1994.

[17] F. A. Kish, D. A. Vanderwater, M. J. Peanasky, M. J. Ludowse, S. G. Hummel, and S. J. Rosner, "Low-resistance ohmic conduction across compound semiconductor wafer-bonded interfaces," *Appl. Phys. Lett.*, vol. 67, pp. 2060–2062, 1995.

[18] G. E. Höfler, D. Vanderwater, D. C. DeFevere, F. A. Kish, M. Carnras, F. Steranka, and I.-H. Tan, "Wafer bonding of 50-mm diameter GaP to AlGalnP-GaP light-emitting diode wafers," *Appl. Phys. Lett.*, vol. 69, pp. 803–805, 1996.

[19] M. R. Krames, M. Ochinai-Holocomb, G. E. Höfler, C. Carter-Coman, E. I. Chen, I.-H. Tan, P. Grillot, N. F. Gardner, H. C. Chui, J.-W. Huang, S. A. Stockman, F. A. Kish, and M. G. Craford, "High-power truncated-inverted-pyramid $(Al_xGa_{1-x})_{0.5}In_{0.5}P$/GaP light-emitting diode exhibiting $>50\%$ external quantum efficiency," *Appl. Phys. Lett.*, vol. 75, pp. 2365–2367, 1999.

[20] R. H. Horng, D. S. Wuu, S. C. Wei, C. Y. Tseng, M. F. Huang, K. H. Chang, P. H. Liu, and K. C. Lin, "AlGaInP light-emitting diodes with mirror substrates fabricated by wafer bonding," *Appl. Phys. Lett.*, vol. 75, pp. 3054–3056, 1999.

[21] R. H. Horng, D. S. Wuu, S. C. Wei, M. F. Huang, K. H. Chang, P. H. Liu, and K. C. Lin, "AlGAInP/AuBe/glass light-emitting diodes fabricated by wafer bonding technology," *Appl. Phys. Lett.*, vol. 75, 1999.

[22] I. Schnitzer, E. Yablonovitch, C. Caneau, and T. J. Gmitter, "Ultra high spontaneous emission quantum efficiency, 99.7% internally and 72% externally, from AlGaAs/GaAs/AlGaAs double heterostructures," *Appl. Phys. Lett.*, vol. 62, pp. 131–133, 1992.

[23] I. Schnitzer and E. Yablonovitch, "30% external efficiency from surface textured, thin-film light-emitting diodes," *Appl. Phys. Lett.*, vol. 63, pp. 2174–2176, 1993.

[24] E. Yablonovitch, T. Gmitter, J. P. Harbison, and R. Bhat, "Extreme selectivity in the lift-off of epitaxial GaAs films," *Appl. Phys. Lett.*, vol. 51, pp. 2222–2224, 1987.
[25] H. W. Deckman and J. H. Dunsmuir, "Natural lithography," *Appl. Phys. Lett.*, vol. 41, pp. 377–379, 1982.
[26] E. Yablonovitch, D. M. Hwang, T. J. Gmitter, L. T. Florenz, and J. P. Harbison, "Van der Waals bonding of GaAs epitaxial liftoff films onto arbitrary substrates," *Appl. Phys. Lett.*, vol. 56, pp. 2419–2421, 1990.
[27] R. Windisch, M. Kuijk, B. Dutta, A. Knobloch, P. Kiesel, G. H. Döhler, G. Borghs, and P. Heremans, "Non-resonant cavity light-emitting diodes," in *Proc. SPIE Photonics West*, 2000.
[28] R. Windisch, B. Dutta, M. Kuijk, A. Knobloch, S. Meinlschmidt, S. S. Chobert, P. Kiesel, G. Borghs, G. H. Döhler, and P. Heremans, "40% efficient thin-film surface-textured light-emitting diodes by optimization of natural lighography," *IEEE Trans. Electron Devices*, 2000.
[29] C. Rooman, R. Windisch, M. D'Hondt, B. Dutta, P. Modak, P. Mijlemans, G. Borghs, R. Vounckx, I. Moerman, M. Kuijk, and P. Heremans, "High-efficiency thin-film light emitting diodes at 650 nm," *Electron. Lett.*, 2001.
[30] W. Schmid, F. Eberhard, R. Jäger, R. King, M. Miller, J. Joos, and K. J. Ebeling, "45% quantum efficiency light-emitting diodes with radial outcoupling taper," in *Proc. SPIE*, vol. 3938, 2000, pp. 90–97.
[31] W. Schmidt, F. Eberhard, M. Schauler, M. Grabherr, R. King, M. Miller, E. Deichsel, G. Stareev, U. Martin, R. Jäger, J. Joos, R. Michailzik, and K. J. Ebeling, "Infrared light-emitting diodes with lateral outcoupling taper for high extraction efficiency," presented at the SPIE Proc. Photonics West, Jan. 1999, San Jose, CA, 1999.
[32] E. M. Purcell, "Spontaneous emission probalbilities at radio frequencies," *Phys. Rev. Lett.*, vol. 69, p. 681, 1946.
[33] E. F. Schubert, Y.-H. Wang, A. Y. Cho, L.-W. Tu, and G. J. Zydzik, "Resonant cavity light-emitting diode," *Appl. Phys. Lett.*, vol. 60, pp. 921–923, 1992.
[34] H. Benisty, H. D. Neve, and C. Weisbuch, "Impact of planar microcavity effects on light extraction—Part I: Basic concepts and analytic tends," *IEEE J. Quantum Electron.*, vol. 34, pp. 1612–1631, Sept. 1998.
[35] ——, "Impact of planar microcavity effects on light extraction—Part II: Selected exact simulations and role of photon recycling," *IEEE J. Quantum Electron.*, vol. 34, pp. 1632–1643, Sept. 1998.
[36] D. L. Huffaker, C. C. Lin, J. Shin, and D. G. Deppe, "Resonant cavity light emitting diode with an Al_xO_y/GaAs reflector," *Appl. Phys. Lett.*, vol. 66, pp. 3096–3098, 1995.
[37] H. D. Neve, J. Blondelle, R. Baets, P. Demeester, P. V. Daele, and G. Borghs, "Resonant cavity LED's," *Microcavities and Photonic Bandgaps: Physics and Appl.*, vol. 324, pp. 333–342, 1996.
[38] K. Streubel and R. Stevens, "250 Mbit/s plastic fiber transmission using 660 nm resonant cavity light emitting diodes," *Electron. Lett.*, vol. 34, 1998.
[39] K. Streubel, U. Helin, V. Oskarsson, E. Bäcklin, and A. Johansson, "High brightness visible (660 nm) resonant cavity light emitting diode," *IEEE Photon. Technol. Lett.*, vol. 10, pp. 1685–1687, Dec. 1998.
[40] M. Jalonen, M. Toivonen, J. Köngäs, P. Savolainen, A. Salokatve, and M. Pessa, "Oxide-confined AlGaInP/AlGaAs visible resonant cvity light-emitting diodes grown by solid source molecular beam epitaxy," in *LEOS 10th Annual Meeting 97*, Nov. 10–13, 1997, pp. 239–240.
[41] M. Dumitrescu, L. Toikkanen, P. Sipilä, V. Vilokkinen, P. Melanen, M. Saarinen, S. Orsila, P. PlSavolainen, M. Toivonen, and M. Pessa, "Modeling and optimization of resonant cavity light emitting diodes grown by solid source molecular beam epitaxy," *Microelectronic Engineering*, vol. 51–52, pp. 449–459, 2000.
[42] R. Wirth, C. Karnutsch, S. Kugler, and K. Streubel, "High efficiency resonant-cavity LED's emitting at 650 nm," *IEEE Photon. Technol. Lett.*, vol. 13, pp. 421–423, May 2001.
[43] H. D. Neve, J. Blondelle, P. V. Daele, P. Demester, R. Baets, and G. Borghs, "Recycling of guided mode light emission in planar microcavity light emitting diodes," *Appl. Phys. Lett.*, vol. 70, pp. 799–801, 1997.
[44] F. Kish, D. Vanderwater, D. DeFevere, D. Steigerwald, G. Hofler, K. Park, and F. Steranka, "Highly reliable and efficient semiconductor wafer-bonded AlGaInP/GaP light-emitting diodes," *Electron. Lett.*, vol. 32, pp. 132–134, 1996.
[45] J. Lacey, D. Morgan, Y. Aliyu, and H. Thomas, "The reliability of (AlGa)InP visible light-emitting diodes," *Qual. Reliab. Engng. Int.*, vol. 16, pp. 45–49, 2000.
[46] M. Watanabe, "High-temperature operation (70°C, 50 mW) of 660-nm-band InGaAlP Zn-diffused window lasers fabricated using highly Zn-doped GaAs layers," *IEEE J. Select. Topics Quantum Electron.*, vol. 5, pp. 750–755, May–June 1999.
[47] H. Tada, A. Shima, T. Utakoji, T. Motoda, M. Tsugami, K. Nagahama, and M. Aiga, "Uniform fabrication of highly reliable, 50–60 mW-class, 685 nm, window-mirror lasers for optical data storage," *Jap. J. Appl. Phys.*, vol. 36, pp. 2666–2670, 1997.
[48] R. W. Herrick and P. M. Petroff, "Improved reliability of red GaInP vertical-cavity surface-emitting lasers using bias-induced annealing," *Appl. Phys. Lett.*, vol. 72, pp. 1799–1801, 1998.
[49] W. J. Choi, J. H. Chang, W. T. Choi, S. H. Kim, J. S. Kim, S. J. Leem, and T. K. Yoo, "Hydrogen effect on 670 nm AlGaInP visible laser during high temperature operation," *IEEE J. Select. Topics Quantum Electron.*, vol. 1, pp. 717–722, June 1995.
[50] K. Endo, K. Kobayashi, H. Fujii, and Y. Ueno, "Accelerated for AlGaInP visible laser diodes," *Appl. Phys. Lett.*, vol. 64, pp. 146–148, 1994.

Klaus Streubel received the Ph.D. degree in physics from the University of Stuttgart in 1991.

In 1991, he took a post-doctoral position at the Swedish Institute of Microelectronics in Stockholm. From 1993 to 1997, Dr. Streubel was employed by the Royal Institute of Technology (KTH), Stockholm as a research stuff member. In 1997, he joined the Optoelectronics department at Mitel Semiconductor AB in Järfälla, Sweden. During this time he was involved in compound semiconductor materials, III–V processing technology and optoelectronic devices. His work included vertical cavity lasers and resonant cavity light-emitting diodes (LEDs), as well as micromachiened optoelectronic components. In 1999, he joined the research and development group at Osram Opto Semiconductors in Regensburg, Germany. His interests now center on InGaAlP-based optoelectronic devices, such as LEDs and lasers. Dr. Streubel has authored or co-authored more than 80 technical papers in international scientific journals, and published some 95 conference papers.

Dr. Streubel is member of the German Physical Society (DPG), the German Society for Crystal Growth (DGKK), and the IEEE LASERS AND ELECTRO-OPTICS SOCIETY (LEOS).

Norbert Linder received the Ph.D. degree from the University of Erlangen-Nürnberg, Germany, in 1996.

From 1996 to 1998, he was a post-doctoral research associate at the University of California, San Diego, where he worked on electron spin dynamics in semiconductor structures. In 1998, he joined the research and development group at OSRAM Opto Semiconductors in Regensburg, Germany. His present interests are the design and development of AlInGaP-based light-emitting diodes (LEDs) and lasers. He has authored or co-authored about 40 technical papers in international scientific journals.

He is a member of the German Physical Society (DPG) and the American Physical Society (APS).

Ralph Wirth received the Ph.D. degree in physics from the University of Stuttgart in 1999, where he worked on modulation properties and gain spectroscopy of AlGaInP lasers and optical anisotropy of spontaneously ordered III/V semiconductors. In 1999 he joined the R&D group at OSRAM Opto Semiconductors in Regensburg, Germany. Of late his field of work covers modeling, design and chip development of AlGaInP-based LED's such as high current, high efficiency and resonant-cavity devices. He has authored or co-authored about 30 conference and technical papers in international scientific journals.

Arndt Jaeger received the diploma degree in physics from the Humboldt-University of Berlin, Germany, and the Ph.D. degree in experimental physics from Philipps-University of Marburg, Germany.

He was a post-doctoral research associate at Max-Born-Institute of Berlin, Germany, City University of New York and University of California at Santa Barbara until joining research and development center of OSRAM Opto Semiconductors at Regensburg, Germany. His present interests involve the optical characterization and study of degradation of optoelectronic devices, in particular AlGaInP light-emitting devices.

Dr. Jaeger is a member of the German Physical Society (DPG).